

A mini guideline study for fly ash-based alkali activated foam masonry units

 C. Kurtulus^a,  M.S. Baspinar^b

a. Dept. of Chemical Engineering, Afyon Kocatepe University, (Afyonkarahisar, Türkiye)
b. Dept. of Metallurgy and Materials Engineering, Afyon Kocatepe University, (Afyonkarahisar, Türkiye)
 cansudemir@aku.edu.tr

Received 10 January 2022

Accepted 16 June 2022

Available on line 13 October 2022

ABSTRACT: This study examined the preparation of fly ash-based foam geopolymer recipes with the experimental design method and data analysis with the SPSS program. A total of 54 prescriptions were used in the studies, which investigated six different variables. Strength, density, and thermal conductivity analyses were performed. Values were in the range of 0.57-2.75 MPa for strength, 344-592 kg/m³ for density, and 0.089-0.132 for thermal conductivity. Three variables were identified with each having the most significant effect on strength and density values. H₂O₂, curing temperature, and expanded perlite had the most effect on strength, while H₂O₂, curing temperature, and alkali concentration had the most significant effect on density. Most influential parameters are plotted on ternary graphs to ensure that the foam concrete (CLC) masonry units used in all types of masonry walls, whether load-bearing or not, can operate under the specified performance conditions.

KEY WORDS: Foam Geopolymer; Experimental Design; SPSS; Masonry Unit.

Citation/Citar como: Kurtulus, C.; Baspinar, M.S. (2022) A mini guideline study for fly ash-based alkali activated foam masonry units. *Mater. Construcc.* 72 [348], e298. <https://doi.org/10.3989/mc.2022.00422>.

RESUMEN: *Un mini estudio de guía para unidades de mampostería de espuma activada con base de cenizas activadas alcalinamente.* Este estudio examinó la preparación de mezclas de geopolímeros de espuma a base de cenizas volantes con el método de diseño experimental y el análisis de datos con el programa SPSS. Se utilizaron un total de 54 prescripciones en los estudios, investigándose seis variables diferentes. Se realizaron análisis de resistencia, densidad y conductividad térmica. Los valores estuvieron en el rango de 0,57-2,75 MPa para resistencia, 344-592 kg/m³ para densidad y 0,089-0,132 para conductividad térmica. Se identificaron tres variables, teniendo cada una el efecto más significativo sobre los valores de fuerza y densidad. El H₂O₂, la temperatura de curado y la perlita expandida tuvieron el mayor efecto sobre la resistencia, mientras que el H₂O₂, la temperatura de curado y la concentración de álcali tuvieron el efecto más significativo sobre la densidad. Los parámetros más influyentes se trazan en gráficos ternarios para garantizar que las unidades de mampostería de hormigón celular (CLC) utilizadas en todos los tipos de muros de mampostería, ya sea que soporten carga o no, puedan operar bajo las condiciones de desempeño especificadas.

PALABRAS CLAVE: Geopolímero de espuma; Diseño experimental; SPSS; Unidad de mampostería.

Copyright: ©2022 CSIC. This is an open-access article distributed under the terms of the Creative Commons Attribution 4.0 International (CC BY 4.0) License.

1. INTRODUCTION

The construction sector is growing at an unprecedented rate around the world, and this trend is anticipated to continue. This rapid growth in the construction industry in recent years, together with the need for technically superior characteristics and values for building materials, has resulted in the use and application of a large number of novel building materials (1). Over the next 40 years, the world is forecast to add 230 billion square feet of new construction, with the building and construction industry accounting for 39% of worldwide final carbon dioxide (CO₂) emissions (2). Concrete, a common construction material composed of aggregates and cement to bind them together, is the third-largest source of human-induced greenhouse gas emissions, behind the transportation industry, for the main pollutant of carbon dioxide in the atmosphere (3–9). Developing enduring construction and building materials with a decreased environmental footprint through both manufacturing and management steps is presently a focal point in the worldwide housing and construction industry (10). As a result of this predicament, it is imperative that sustainable alternatives to cement and building materials containing cement be utilized in construction in order to preserve the long-term viability of the environment (11). The Paris Climate Agreement, which was signed in 2015, also requires all countries to adhere to the emission targets specified (12).

Alkali-activated materials (AAM), generally called geopolymers, are a relatively new class of attractive construction material that offer a solution to limit the adverse results of cement manufacturing. These materials are gaining popularity due to their environmental and performance advantages over standard Portland cement concrete and cement-based construction materials (13). Alkali activated concretes (AAC) have become an issue of great importance due to their widely accepted identification as “environmentally friendly” or “green” construction materials compared to cement-based concretes due to their low CO₂ emission potential and ensuring recycling of industrial by-products (14–18). There are many groups in the scientific and commercial communities trying to improve new binders with the alkaline activation of industrial by-products (3–8).

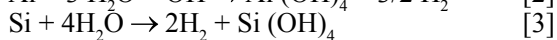
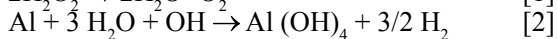
The term geopolymer was first used by the French scientist Joseph Davidovits to measure the tridimensional structure of inorganic polymers, which are formed by low-temperature polycondensation of aluminosilicates (19). There are a wide variety of potential solid aluminosilicate raw materials for the synthesis of inorganic polymers such as fly ash, blast furnace slag, metakaolin, construction and demolition wastes, and red mud (19–22). Geopolymer-based inorganic materials have a wide variety

of application areas, including fire-resistant materials, thermal insulation, building materials, water purification, and so on (19, 23, 24).

Masonry units are an ancient and fundamental construction and building material used all over the world. Earth masonry units (adobe or compressed earth blocks) account for a significant portion of the built environment today. Earth-based buildings house from one-third to half of the world’s population (25) mainly for houses and apartment buildings. These construction technologies are extensively employed world-wide both in developed and developing countries, sometimes due to strong cultural aspects, long time tradition or even as a symbol of solid construction. Moreover the good performance of masonries is well known by the users, including its strength, thermal and acoustical properties. In developing countries besides the former reasons, brickwork or blockwork are the only suitable methods for self-construction in non-industrialized circumstances. However the traditional masonry units are usually non-eco-friendly products, mainly because of their high energy consuming components due to their production method (fired-clay bricks. Bricks can be composed of a variety of materials, including calcium silicate, concrete, and clay, while clay and concrete bricks are the most common. Clay brick manufacture, on the other hand, necessitates high-temperature (900-1000°C) kiln burning, which emits a significant amount of greenhouse gases (26). According to the World Business Council for Sustainable Development Agency (2017) and the cement technology roadmap by 2050 research, the contribution of ordinary Portland cement (OPC) production worldwide to greenhouse gas emissions is estimated to be approximately 1.35 billion tons annually or approximately 7% of the total greenhouse gas emissions into the earth’s atmosphere (27). In light of all this information, sustainable concretes should be created with readily available resources on earth, recycled materials with low energy requirements, and generated with little or no waste, in order to have the least possible environmental impact (28–30). Mined raw materials and non-renewable energy are used in the cement industry. The utilization of industrial by-products can greatly reduce the amount of energy used in these processes, as well as waste management. Through the use of waste materials, geopolymer technology reduces greenhouse gas emissions and lowers raw material costs (11, 31).

Economic and environmental restrictions are becoming more prevalent nowadays, and one of the implications for the construction sector will be a demand for more energy-efficient building and construction materials (32). When it comes to energy leaks in buildings, it’s estimated that the walls account for about 40% of the heat loss (33–35). When masonry units (adobe bricks or compressed earth blocks) used as construction wall elements are examined for thermal insulation, it is well known that they have very

low results. Thermal insulation materials are the most powerful approach to reducing heat loss from buildings, hence diminishing heat energy requirements and contributing to the near-zero energy objective (36). As a result, insulating materials are required in addition to construction materials. Despite XPS and EPS providing excellent insulation and having extremely low-density values, their limited fire resistance makes them unsuitable for use in buildings. Aside from the fact that glass wool and stone wool are useful in terms of density, thermal insulation, and non-flammability, the materials employed for bonding during application cause non-flammability to be compromised (37–40). Polystyrene and polyurethane are also poisonous, and they release poisonous smoke when they burst into flames (41). Geopolymer foams have drawn the attention of researchers and studies were carried out for many years due to better properties (thermal stability, inflammability, and green production process) compared to conventional building insulation materials (42–46). Wall elements with thermal insulation capabilities must have high closed porosity, low density, and low water absorption to achieve the necessary thermal insulation performance (47). Aside from that, lightweight masonry modules are frequently used in the construction sector to reduce dead load and improve earthquake safety. Although density values range from 300 to 2000 kg/m³ depending on the application, those with a density of 300–1200 kg/m³ are favored, with a strength value of 1–100 MPa desired (48). For the foaming of lightweight geopolymer foams, the direct foaming approach was recommended in various research (44, 49–52). Porous materials are created by adding air into a suspension or liquid medium through direct foaming processes. The amount of gas contained in the geopolymer slurry influences overall porosity, and pore size is linked to setting characteristics (53). The size and distribution of the cured foams are influenced by the blowing agent used and the amount added (54). Foaming is commonly accomplished by mechanically mixing H₂O₂ (49), metallic Al (40), metallic Si (55), and sodium perborate (56) into the geopolymer sludge. The degradation of the additives in the alkaline sludge results in the formation of a bubble and a porous layer. In Equations [1], [2], and [3], a bubble and porous structure are created because of the degradation of the additives in the alkaline sludge:



Due to the general high gas-liquid contact area, liquid foams are thermodynamically unstable. As a result, several physical processes like drainage, creaming, and Ostwald ripening destabilize the slurry, causing large pores to form. Surfactants are required to maintain system stability, manage the pore

size distribution, and lower the angle at the gas-liquid interface. Surfactants keep gas bubbles stable in the system by preventing them from aggregating. Surfactants such as butyric acid, valeric acid, butyl gallate, propyl gallate, hexylamine, and calcium stearate are commonly utilized (57–62).

Another technique to improve energy efficiency in buildings is to incorporate lightweight aggregates to increase porosity and acquire low density construction material at the same time. One of the materials used for this is expanded perlite (49, 63–65). Expanded perlite is a siliceous volcanic glass with a large volume that expands significantly when heated. Its volume grows 4–20 times when heated above 870 °C (66). The thermal insulation qualities of expanded perlite are greatly improved as a result of this increase in volume and porous structure. Furthermore, compared to the density of conventional perlite, expanded perlite has very low density. Compared to alternative materials including exfoliated vermiculite, expanded clay or shale, pumice, and mineral wool, the low cost of expanded perlite may be a significant advantage (65).

The current consensus is that there are many variables affecting the properties and performances of fresh and hardened geopolymeric materials, including alkaline concentration, curing temperature, curing duration, Na₂O/SiO₂ ratio, SiO₂/Al₂O₃ ratio, H₂O/Na₂O ratio, and additives (19, 67–69). Although many studies were performed about improving the mechanical properties of geopolymer materials and geopolymer foams, different foam forming methods (49, 70, 71), stabilizing foam cells (72, 73), and examining the thermal properties of geopolymer foams (61, 74), there are no guidelines and comprehensive publications examining the mechanical, physical and thermal properties of many samples.

So far, investigations of alkali activated materials generated utilizing slag and fly ash as raw materials has continued, significantly in relation to microstructures, workability, mechanical performance, and durability (17, 75, 76). Alkali activated materials were used in some real situations in Asia, Australia, and Europe with established technical specifications (1, 14, 15). Nevertheless, due to a shortage of clear guidelines that may be extensively recognized, alkali activated blend formulation is almost always difficult to evaluate and recreate. For this reason, determining the working range with a detailed study is important research for alkali activated concrete. The properties and necessary performance conditions of foam concrete (CLC) masonry units used in all types of masonry walls, whether load bearing or not, are presented in TS13655 (Turkish Standard). According to this standard, the strength value of all kinds of walls, including monolithic walls, sandwich (double-layer walls) walls, partition walls, retaining walls and foundations, as well as general applications underground, should be >1 MPa and <450–550 kg/m³ density property.

Experimental design methods have gained popularity in recent years for various reasons, including obtaining more information with less laboratory effort, saving time and raw materials, and examining the variables that influence the critical attributes. When an investigation is conducted without employing the experimental design approach, modifications are made to the first variable assumed to influence the outcome, and the first variable is used until the best values are found. When trying to find the best values for the second variable, there will be a shift from the first variable's optimum value. Every modification performed at the variable level will lead to changes at all levels. Although the influence level of each variable will be understood separately, the process will not be fully understood, and the effects of the variables on one another will not be resolved. The effect of one variable can be evaluated with varying degrees of other variables in studies that follow the experimental design method, and more data can be gathered with fewer experiments (77, 78).

For the subject of geopolymers, there are many researchers who obtained findings using different experimental design methods. In their studies, they generally focused on critical parameters such as water/binder ratio, fly ash/alkali ratio, alkaline concentration, and raw material ratio. Li *et al.* worked on slag-based concrete using the Taguchi method (79). In addition, Nazari *et al.* prepared geopolymers containing rice husk ash and fly ash using the Taguchi method and determined the optimum mix compositions (80). Hadi *et al.* conducted studies on geopolymer-based concretes using the multiple regression model with four variables related to strength and slump set time, and developed formulations including alkali /binder, sodium silicate/sodium hydroxide, and water/binder ratios (81). Lokuge *et al.* studied fly ash-geopolymer concrete using a multivariate adaptive regression spline model. During their studies, they collected all the literature on the subject and analyzed the variables of water/binder, alkali/binder, sodium silicate/sodium hydroxide, and alkaline concentration (82). Onoue *et al.* performed an experimental design about fly ash-based geopolymers using the Taguchi method. They studied the sodium silicate/sodium hydroxide ratio, alkaline concentration, fly ash-slag ratio, mixing time, curing temperature, and cumulative temperature with two different fly ash types purchased from different lots (83).

This article presents comprehensive results about the physical properties, mechanical properties, and thermal conductivity properties, which will guide the preparation phase of fly ash-based geopolymer foams that are planned to be used as building materials. This study is also crucial in terms of evaluating fly ash, which is a thermal power plant waste, in the context of the circular economy and transforming it into a value-added product in the field of construction.

2. MATERIALS AND METHODS

Solid main raw materials used for the preparation of foam geopolymers are fly ash and metakaolin. Fly ash was supplied by Seyitömer Thermal Power Plant (Kütahya/Turkiye). It is classified as Class F according to the ASTM-C618 (84). Metakaolin powder (MEFISTO L05) was purchased from the Czech Republic. Sodium silicate solution and sodium hydroxide particulates were used in the preparation of alkaline solution. In the foam formation phase, hydrogen peroxide (30% concentration) was used as a foaming agent. and calcium stearate was used as a surfactant. Additionally, chopped polypropylene fiber (1 cm long and 30 μm diameter) and expanded perlite (1-3 mm diameter) were added to samples. To improve the geopolymerization properties of the solutions, a small amount of metakaolin was added. To abide by the circular economy goal while also improving geopolymerization, a maximum of 15% metakaolin was added (85, 86). Calcium stearate was chosen due to its outstanding surfactant properties while being affordable, odorless, and having low toxicity (87). It is a white powder, that is slippery and insoluble in water. Chopped polypropylene fiber was added to the samples to prevent cracks that may occur during drying (88–94), and expanded perlite was added to improve the thermal insulation properties (49, 63, 65, 95).

Table 1 summarizes the chemical compositions of solid raw materials measured by XRF, and Table 2 gives specific surface area and specific weight of raw materials, respectively. The specific surface area of fly ash and metakaolin were detected by the BET method. Density values of aluminosilicate raw materials were measured with a pycnometer.

In order to prepare the alkaline solution, NaOH plates were completely dissolved in sodium silicate solution. To ensure the homogeneous distribution, the fibers added to the alkaline mixture were mixed for

TABLE 1. Chemical composition of aluminosilicate raw materials.

	SiO ₂	Al ₂ O ₃	CaO	Fe ₂ O ₃	MgO	K ₂ O
Fly Ash (%)	50.30	19.10	4.55	12.40	4.67	2.16
Metakaolin (%)	54.10	41.10	0.13	1.10	0.18	0.80

TABLE 2. Physical properties of aluminosilicate raw materials.

Properties	Fly Ash	Metakaolin
Specific Surface Area (kg/m ²)	7.91	17.08
Density (kg/m ³)	2.58	2.50

another one minute. Solid content was homogeneously mixed by adding calcium stearate into the mixture containing metakaolin and fly ash. The alkaline solution was poured onto the solid mixture without waiting for it to cool and the geopolymer content was mixed for five minutes. After that, H₂O₂ was added to the geopolymer mixture and the blend was mixed vigorously for 1 minute. Finally, the geopolymer mixture was poured into 10x10x10 cm molds and cured for 24 hours in an oven (Figure 1). The hardened geopolymers were demolded and stored at room temperature for 28 days.

The samples prepared for thermal conductivity analysis were produced as presented in the flow chart in Figure 1. Since the authors preferred the guarded hot plate method for thermal conductivity analysis, the samples were produced with 30x30x5 cm dimensions.

Compressive strength, bulk density, and thermal conductivity analyses of the prepared foam samples were performed on the 28th day. Analysis of the large amount of data obtained was performed with the SPSS program, and the results obtained were confirmed with statistical data.

2.1 Experimental design procedure

Geopolymer experiments were conducted with Box Behnken experimental design method. A detailed study was carried out to obtain comprehensive information about compressive strength, density, and thermal conductivity properties of fly ash-based foam geopolymers. The maximum (1), minimum (-1) and average (0) values for six variables were determined for the experiment design. Maximum and minimum values were provided by using preliminary studies. The average value (0) represents the mean of the maximum and minimum value. The values determined for the experiment design are presented in Appendix 1. Oxide molar ratios of all mix design compositions of samples are shown in Table 3. Contour plots were used to interpret the complex data collected.

2.2 Instrumentation

Compressive strength was tested with 10x10x10 cm specimens. Samples were cured at room temperature (25 °C±1 and 50±5% relative humidity) for 28 days. The strength of geopolymer foams was tested with a loading rate of 3 kN/s. Bulk densities of samples cured at room temperature for 28 days were measured in accordance with ASTM C642. At least three samples were examined, and average values were recorded. Scanning electron mi-

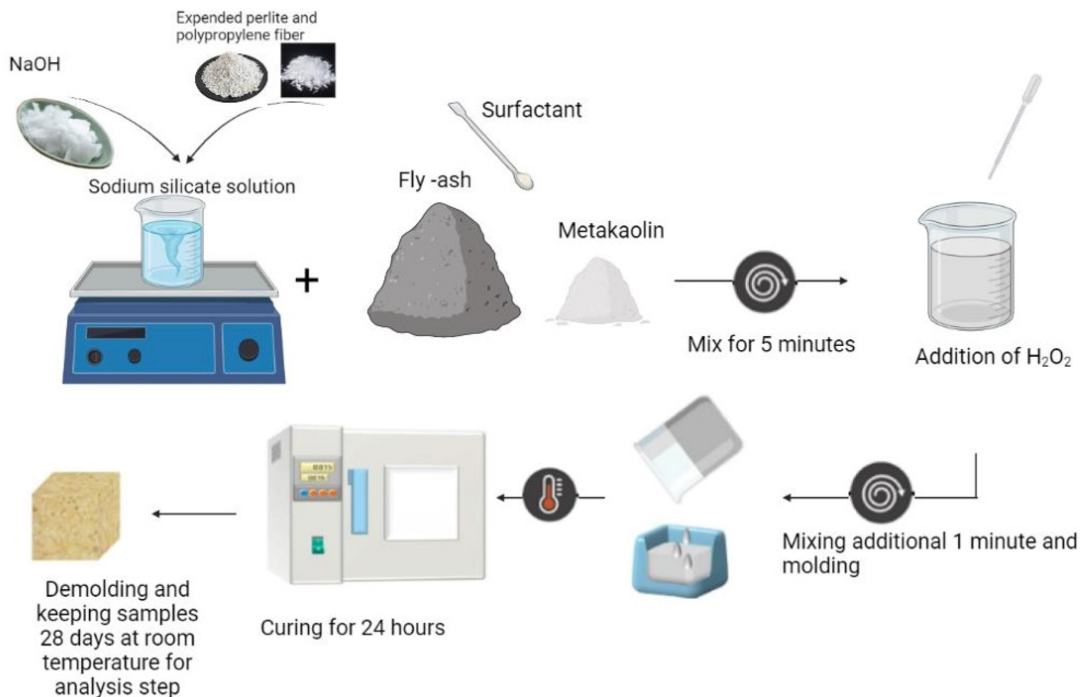


FIGURE 1. Schematic presentation of the synthesis of fly ash-based porous geopolymers.

TABLE 3. Oxide molar ratios of geopolymer pastes.

Fly Ash-Metakaolin Ratio (%)	Alkaline Concentration	H ₂ O/Na ₂ O	SiO ₂ /Al ₂ O ₃	Na ₂ O/SiO ₂	Na ₂ O/Al ₂ O ₃
85-15	6M	13.42	5.19	0.28	1.40
	8M	11.75	5.19	0.33	1.63
	10M	10.47	5.19	0.37	1.85
90-10	6M	13.40	5.44	0.28	1.47
	8M	11.73	5.44	0.33	1.71
	10M	10.45	5.44	0.37	1.95
95-5	6M	13.37	5.72	0.28	1.55
	8M	11.71	5.72	0.33	1.80
	10M	10.44	5.72	0.37	2.05

croscopy (SEM) with back-scattered electron (BSE) images were performed to analyze the surfaces of the specimens and investigate porosity on a LEO 1430 VP device. Secondary electron images were obtained with an acceleration voltage of 20 kV. Information about bonds formed in geopolymer samples and their amounts were obtained by the FTIR method. FTIR analysis was performed to correlate with drying shrinkage. The samples were characterized by diamond ATR spectroscopy and absorption spectra in the 4000-400 cm⁻¹ spectrum range. The thermal conductivity of samples was tested using a TA Instruments FOX 314 Thermal Conductivity Analyzer. The guarded hot plate method was used to measure the thermal conductivity of low conductivity construction and insulation materials at a temperature of 25 °C. The samples were dried in an oven at 105 °C until they attained a consistent weight for thermal conductivity analysis.

All samples were subjected to strength and density tests. Thermal conductivity investigation was done on samples chosen from among those that showed the best strength and density performance. As a result of these analyses, contour plots were created. Only selected samples were subjected to XRD, SEM and FTIR analyses. The formulations of the selected samples are depicted in the figures that accompany the analysis findings.

3. RESULTS AND DISCUSSION

3.1 Compressive strength analysis

In the study, the effects of all variables on strength were examined with the help of contour graphics and the results are presented in Table 4 and Figure 2. As

the indicator on the right side of the graphics turns from cold colors to warm colors, the strength value increases. As shown in all figures, the strength values vary between 0.57 MPa and 2.75 MPa. The graphs with the most transitions between colors were examined visually, and H₂O₂, expanded perlite, and curing temperature were the variables that have the most effect on strength.

Data obtained from compressive strength tests were analyzed using statistical analysis methods. Multiple regression was carried out with the help of stepwise linear regression in order to investigate which variables used in geopolymer composition contributed more to strength development (Table 4). Stepwise linear regression is a method of regressing multiple variables while simultaneously removing those that aren't important. SPSS ordered the variables in the model according to their correlation strengths with the dependent variable, as shown in Table 4. The model was constructed by measuring the effect of each variable entered into the model. The model shows that H₂O₂, curing temperature, alkaline concentration, and expanded perlite amount all influenced strength. The beta value describes the effect of the independent variable on the dependent in multiple regression. Regardless of sign, large numbers represent the most impactful parameter on the property. The relative importance of the variables on strength, according to the standardized regression coefficient (β), were H₂O₂ amount, curing temperature, alkaline concentration, and expanded perlite quantity. H₂O₂ and expanded perlite were negatively connected to strength and strength was positively related to curing temperature and alkaline concentration. A positive relationship suggests that the change is directly proportional, while a negative relationship shows that the change is inversely proportional. When the significance (p-value) of the

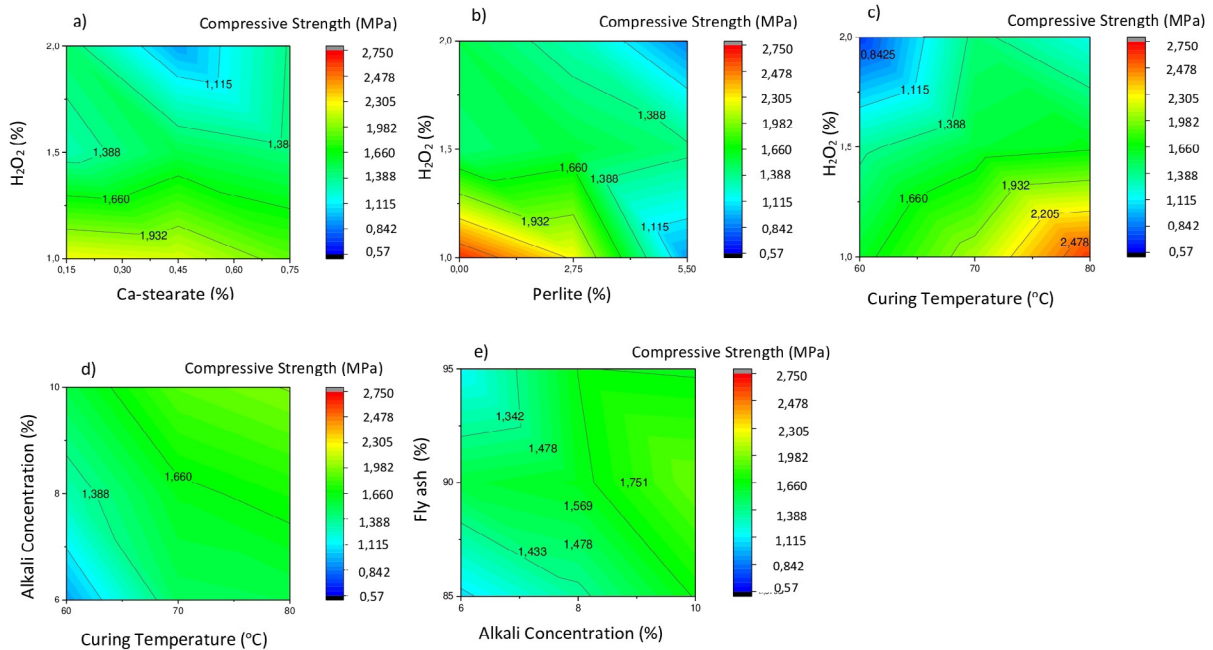


FIGURE 2. Contour charts of all measured strength values. a) Hydrogen peroxide vs. calcium stearate b) Hydrogen peroxide vs. perlite, c) Hydrogen peroxide vs. curing temperature vs., d) Alkaline concentration vs. temperature e) Fly ash vs. alkaline concentration.

TABLE 4. Statistical analysis of variable data thought to affect strength.

Model	B value	Standard Error	Beta value	p-value	R ²	Binary r
Constant	0.614	0.767				
H ₂ O ₂ (%)	-0.779	0.177	-0.479			-0.624
Curing Temperature (°C)	0.022	0.009	0.269	<0.001	0.424	0.518
Alkaline concentration (M)	0.101	0.044	0.248			0.340
Expanded Perlite (%)	-0.073	0.032	-0.248			-0.616

variables and models is assessed, the association between the variables was statistically significant because the values are less than 0.05.

The negative and moderate value ($r=-0.624$) correlation between H₂O₂ and strength values was obtained using binary correlations between the strength value and the variables. The curing temperature and strength values were found to have a positive and moderate binary ($r=0.518$) correlation. The alkaline concentration and strength values were found to have a moderate ($r=0.340$) positive binary interaction. Finally, a moderate binary ($r=0.616$) negative association was calculated between expanded perlite content and strength development.

The table shows that H₂O₂ and expanded perlite reduce strength, whereas curing temperature and alkaline concentration enhance strength. The numerical size of the beta value, regardless of sign, also provides

the most information about the effect of variables on strength. This means that H₂O₂, curing temperature, alkaline concentration, and expanded perlite all impact compressive strength.

In this context, the authors created a ternary strength graph by selecting three different variables that have the greatest impact on strength. In this case, the authors chose three variables that had the greatest impact on strength and created a ternary strength graph to estimate the operating range.

The area covered by red, yellow, and green on the triangle graph suggests that strength values at and above the intended value (1 MPa) can be obtained, which was determined at the start of the study. As an outcome, samples made at maximum 1.0% H₂O₂, minimum 70 °C, and containing any amount of expanded perlite can achieve >1.0 MPa strength. The coloring changes to turquoise and dark blue in loca-

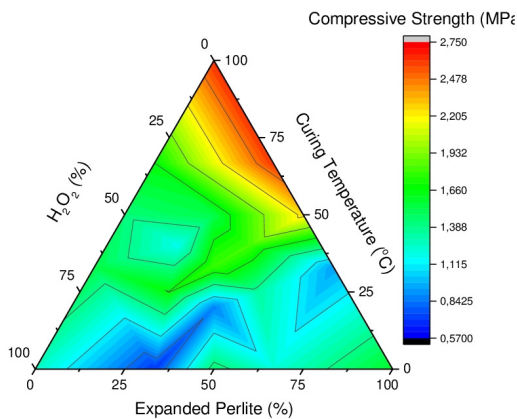


FIGURE 3. Presentation of the most effective variables on strength in ternary graphs and working range detection. (Values used in the study were normalized out of 100 among themselves. So 0=1.0%, 50=1.5%, 100=2.0% for hydrogen peroxide, 0=60 $^{\circ}C$, 50=70 $^{\circ}C$, and 100=80 $^{\circ}C$ for the curing temperature, and 0=0%, 50=2.75%, 100=5.5% values for expanded perlite amount).

tions where the curing temperature is lower than the established value and the H_2O_2 amount is higher than the indicated value, where strength values below the target value are feasible.

While the maximum compressive strength was achieved at 80 $^{\circ}C$, the minimum compressive strength was obtained at 60 $^{\circ}C$, and the strength gradually varied as the temperature was increased. The compressive strength increased when the curing temperature was raised, according to this finding. Although Hardjito et al. (96) asserted that increasing the curing temperature over 60 $^{\circ}C$ does not considerably increase compressive strength, temperature increased strength in fly ash-based geopolymer foams in our work.

The degree of porosity mainly controls the mechanical strength of the geopolymer foam (55). The increase in H_2O_2 contributes to thinning and weakening of the pore walls and decreasing bulk density values cause a decrease in strength. Geopolymer foams containing 1.0% H_2O_2 reached a strength value of >2.5 MPa. While the strength values of samples containing 1.5% H_2O_2 decreased to 1.5-2.0 MPa, it even falls below 1.0 MPa for samples containing 2.0% H_2O_2 .

When expanded perlite is added to a geopolymer mixture, its porous and weak structure causes weak zones (97). As a result, expanded perlite in the combination has a negative impact on the mechanical characteristics. While samples without any expanded perlite can reach a strength value of about 1.5 MPa, when 2.5% expanded perlite is added to the mixture, the strength value drops from one to 0.5 MPa.

Using the triple chart in Figure 3, H_2O_2 must be less than 1.5%, curing temperature must be greater than 70 $^{\circ}C$, and perlite must be less than 2.75% to achieve strengths greater than 1 MPa required by the TS13655 standard.

3.2 Density analysis

The findings for density analysis are shown in Appendix 1, statistical results in Table 5, and the contour plots in Figure 4 were utilized to observe the variables that affect sample densities. Figure 4a reveals that, regardless of the amount of calcium stearate used, sample densities vary directly with the amount of hydrogen peroxide. Figure 4b shows that hydrogen peroxide has a greater effect on density values than expanded perlite. The density values were somewhat affected by the temperature increase in Figures 4c and 4d, and the density values may increase with the increase in alkaline concentration. Figure 4e demonstrates that the amount of fly ash has little effect on the density values.

Multiple regression was performed using the stepwise linear regression approach, as in the compressive strength study, to determine the variables impacting the density of the foam geopolymers. Table 5 shows the parameters that have the greatest impact on density. The most effective variables on density in this model were peroxide, curing temperature, and alkaline concentration. When the significance (p-value) of the variables and models presented in the table are examined, the relationship between the variables was statistically significant since the values are less than 0.05. Along with low density, expanded perlite is commonly used in manufacturing lightweight concrete (98, 99). Even though expanded perlite was employed in the study, it was not one of the variables affecting density in the SPSS analysis. The small amount in the composition is considered the main cause. As a result, as can be followed by the beta values, hydrogen peroxide, curing temperature, and alkaline concentration all had a greater impact on the density value, respectively.

As presented in Table 5, the variables of hydrogen peroxide, curing temperature, and alkaline concentration had a significant and robust relationship ($R^2=0.874$ and $p<0.05$). Together, these three variables explain approximately 87.4% of the total variance of the density values. There was a negative and robust ($r=-0.789$) relationship between H_2O_2 and density values. There was a positive and low binary correlation ($r=0.177$) between the curing temperature and the density values. A moderate ($r=0.332$) positive binary correlation was calculated between alkaline concentration and density values. Thanks to model three, a ternary diagram was drawn, and the operating range was determined by considering the parameters that most affected the density value (Figure 5).

Although Hardjito et al. (100) claimed that raising the curing temperature above 60 $^{\circ}C$ does not increase the compressive strength significantly, in this study, the temperature increased the strength of fly ash-based geopolymer foams.

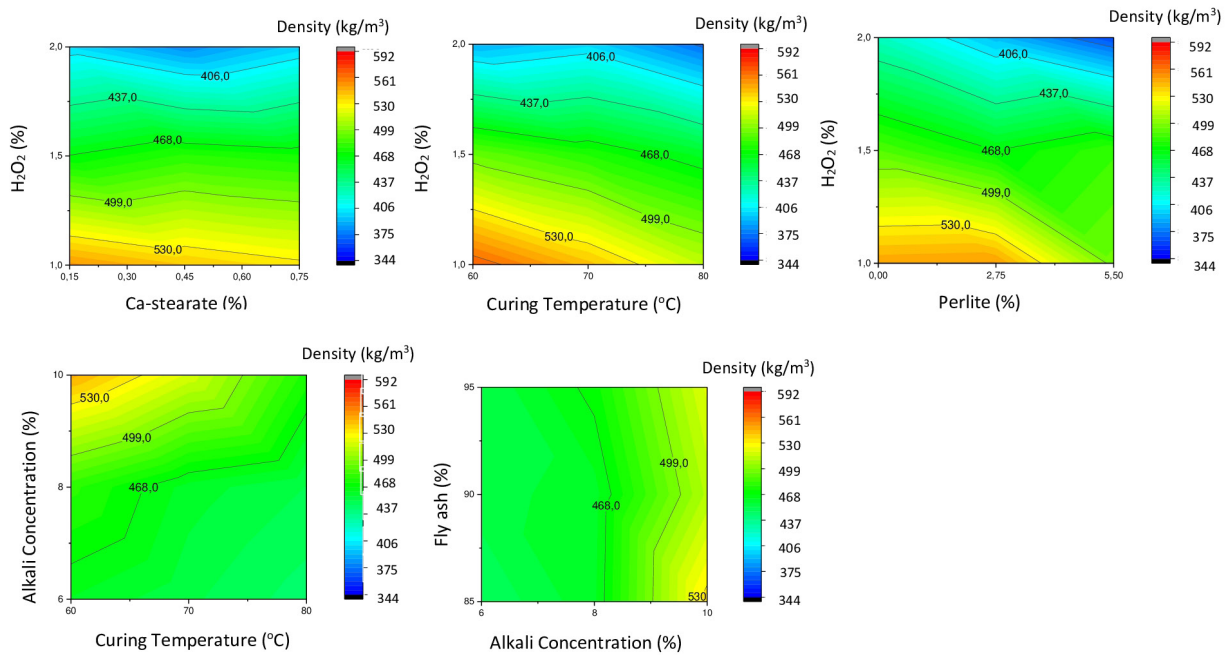


FIGURE 4. Contour charts of measured density values. a) Hydrogen peroxide vs. calcium stearate b) Hydrogen peroxide vs. perlite, c) Curing temperature vs. hydrogen peroxide, d) Curing temperature vs. alkaline concentration, e) Fly ash vs. alkaline concentration.

TABLE 5. Statistical study of variable data to help determine density.

Model	B value	Standard Error	Beta value	p-value	R ²	Binary r
Constant	687.370	56.011				
H ₂ O ₂ (%)	-148.667	12.983	-0.788	0.000	0.874	-0.789
Alkaline concentration (M)	15.667	3.246	0.332			0.332
Curing Temperature (°C)	-1.667	0.649	-0.177			0.177

To produce a sample with the density of 450-550 kg/m³ required by the TS13655 standard, the triple graph in the figure indicates that H₂O₂ must be less than 1.75%, curing temperature must be higher than 70 °C, and alkaline concentration must be greater than 8 M.

3.3 Thermal conductivity analysis

The Figure 6 shows contour plots created from the thermal conductivity analysis findings. The thermal conductivity values of fly ash-based geopolymer foams ranged between 0.089 to 0.1328 W/mK, according to the results of the investigation. The effect of H₂O₂ and Ca-stearate on thermal conductivity is seen in Figure 6a. Ca-stearate and H₂O₂ both appear to improve the insulating capabilities gradually. The decrease in heat conductivity was induced by the presence of more air gaps in the geopolymer matrix caused by the

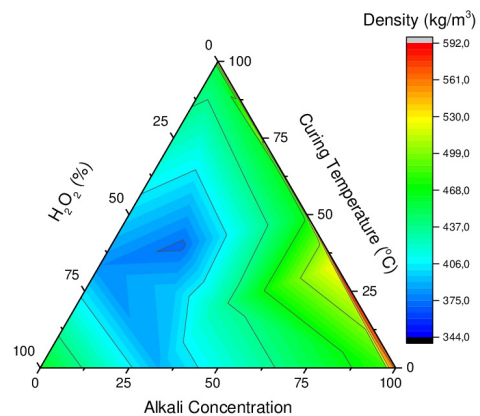


FIGURE 5. Presentation of the most effective variables on density in ternary graphs and determination of working range. (Values used in the study were normalized out of 100 among themselves. So 0=1.0%, 50=1.5%, 100=2.0% for hydrogen peroxide, 0=60°C, 50=70°C, and 100=80°C for the curing temperature, and 0=6 M, 50=8 M, 100=10 M values for alkaline concentration).

increased amount of H_2O_2 (39, 101, 102) and the reduction of pore diameters generated by Ca-stearate (73, 103–105) in the composition. The effect of fly ash and calcium stearate on thermal conductivity is seen in Figure 6b. The amount of fly ash was found to influence thermal conductivity, initially decreasing and later boosting it. Figure 6c demonstrates that when the alkali concentration increases, the thermal conductivity values drop; however, the expanded perlite additive enhances insulation. The thermal insulation qualities of the structure increased because expanded perlite enhances the total porosity of the structure (65, 106). The thermal conductivity value is thought to increase when the alkali content in the geopolymer density values rises (107, 108).

3.4 SEM analysis

Figure 7 presents the microstructure properties of the synthesized fly ash-based geopolymers as evaluated by SEM. The microstructure of foam geopolymers generated with different concentration levels of alkaline activator is shown in Figures 7a–7b. Increasing concentrations of alkaline activator create more pores and reduce the pore sizes in the areas examined at equal magnifications. The viscosity of the geopolymer mixture increases as the alkalinity rises. The increased exter-

nal pressure around the pores inhibits their growth and development (34, 109). As a result, the pores formed in geopolymer compositions with lower alkalinity are smaller. In Figure 7c-7d, the pore size of the foam geopolymer grows as the amount of H_2O_2 increases. As the amount of dissociated O_2 increased in tandem with the amount of H_2O_2 , the pores enlarged and more porosity occurred (49). The pore size distribution in geopolymer foams at different foaming temperatures is shown in Figures 7e and 7f. As the foaming temperature increased, the number of large pores reduced, and the distribution of pores became more uniform. The fundamental reason for this is that as the temperature goes up, the geopolymerization process accelerates, and the gas generated as a result of the decomposition of H_2O_2 in the composition remains trapped in the structure as it begins to harden and is unable to join with other pores and expand (110). Figure 7g presents scanning electron microscopy images of the geopolymer containing expanded perlite, which appears to have high porosity. Expanded perlite, which has high porosity, is exceptionally light, and it is inevitable that it causes a severe decrease in density depending on the amount added to the final product (65). Excess expanded perlite content, which has low strength, in the mixture causes deterioration in the mechanical properties of the final product, as it will cause the formation of porous and low strength areas.

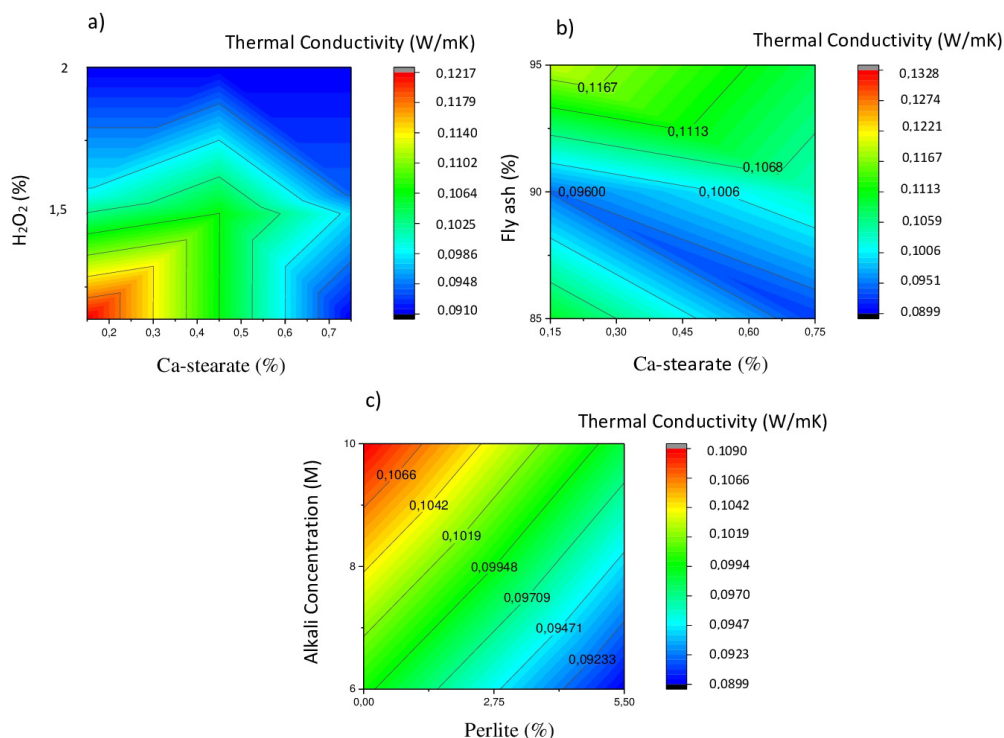


FIGURE 6. Contour charts for measured thermal conductivity values. a) Hydrogen peroxide vs. calcium stearate, b) Fly ash vs. calcium stearate, c) Alkali concentration vs. perlite.

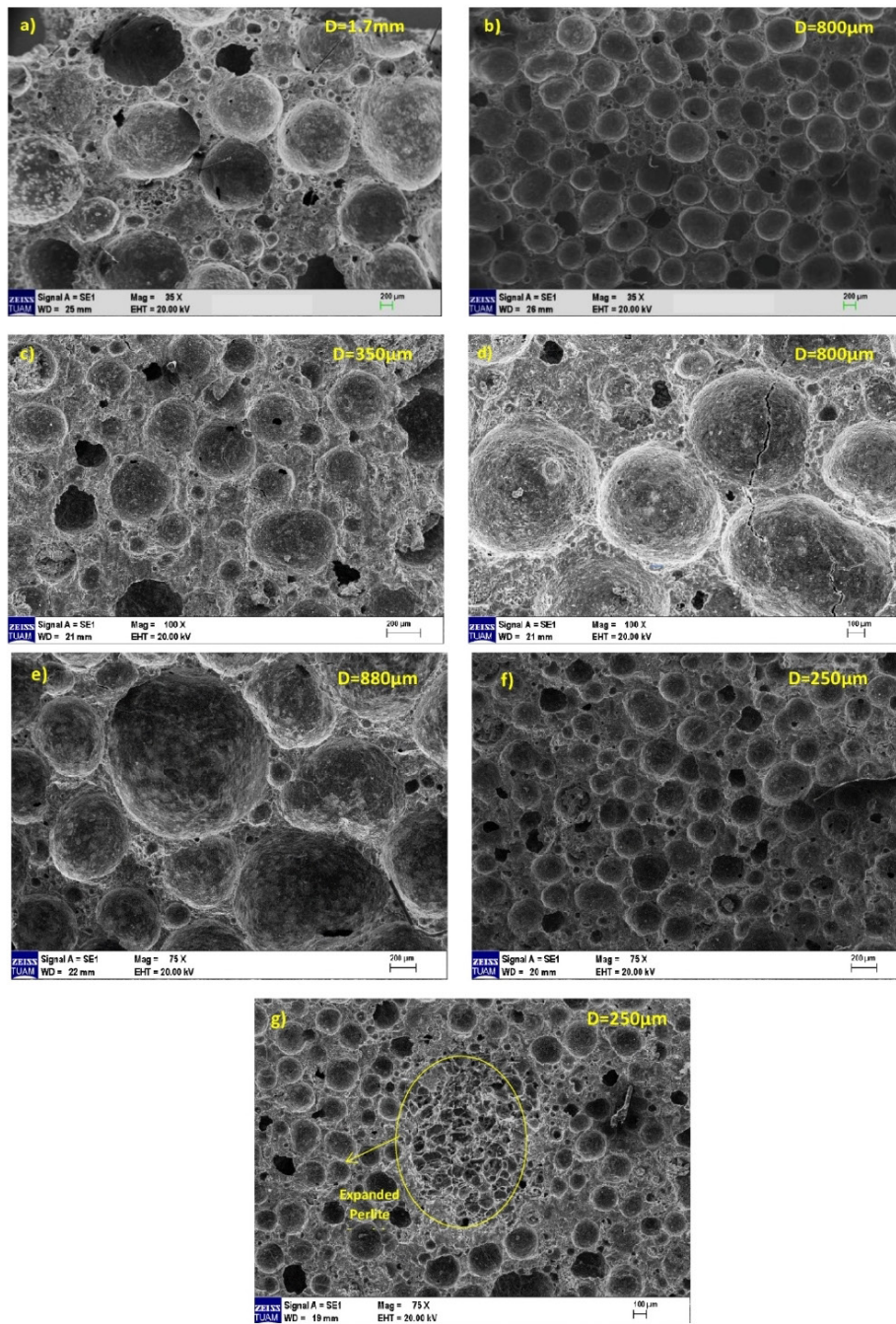


FIGURE 7. SEM Images of geopolymer samples. a) 6M-90UK-0.15CS-70C-7H₂O₂ b) 10M-90UK-0.15CS-70C-7H₂O₂ c) 8M-90UK-0.15CS-70C-4H₂O₂ d) 8M-90UK-0.15CS-70C-7H₂O₂ e) 10M-90UK-0.45CS-60C-5.5H₂O₂ f) 10M-90UK-0.45CS-80C-5.5H₂O₂ g) 10M-90UK-0.45CS-80C-5.5H₂O₂.

3.5 FTIR analysis

The influence of curing temperature, alkali concentration and aluminosilicate raw material combinations on the structural alterations and reaction products of fly ash-based foam geopolymers was investigated using FTIR experiments. For the FTIR study, a Bruker Vertex 70V type spectrom-

eter device (400-4000 cm⁻¹) was used. The results of FTIR spectroscopy are represented graphically as transmittance vs. wavenumber. The spectra lines of foam geopolymer samples are shown in Fig. 7. The H-OH bending and -OH symmetric and asymmetric stretching functional groups are apparent in the broad and strong peaks at 3600-3000 and 1650 for foam geopolymer samples. The water and poten-

tial -OH groups in the oligomeric solute species are responsible for these bands. The significant peaks detected in FTIR analyses of geopolymers between 1000 and 600 cm^{-1} are known to be connected with asymmetric vibrations of T–O–Si bonds (T = Si or Al) (111). The peak at 970–800 cm^{-1} is linked to Al–O–Si bond bending vibrations, while the peak at 420 cm^{-1} is linked to Si–O–Si bending vibrations (112). The slight changes in the wavenumber 2200–1800 cm^{-1} detected in the geopolymer compositions with added organic surfactant reveal the symmetrical and asymmetrical vibrations of CH_2 due to the organic surfactant component (113). In addition, carbonyl stretching peaks (COO-) from the chemical structure of Ca-stearate were detected at 1600 cm^{-1} . The peak for the Si–O–Ca vibration can be seen at 750 cm^{-1} (114).

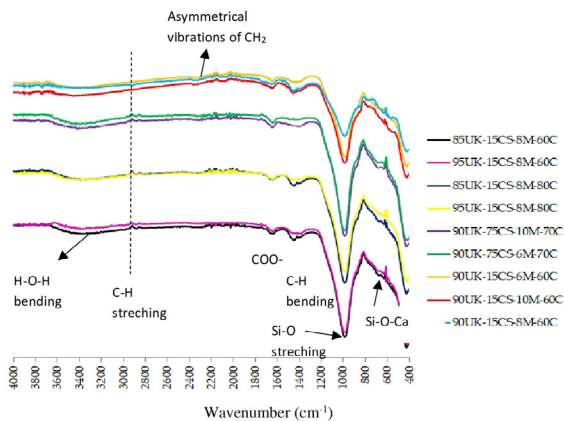


FIGURE 8. FTIR studies of geopolymer foam compositions. (Abbreviations: UK: Fly ash, CS: Calcium stearate, M: Alkaline Concentration, C: Degrees Celsius).

3.6 XRD analysis

Figure 9 shows the results of X-ray diffraction investigations of geopolymer foam samples. The examination results for all fly ash-based samples revealed the presence of quartz phase. The effects of varying the amount of fly ash, alkaline concentration, and the curing temperature were all noticed. The characteristic hump ($2\theta = 20\text{--}40^\circ$) of amorphous gels was detected due to the creation of a geopolymer structure generated during the dissolution of the fly ash glassy phase (62, 115). Because the regions beneath the characteristic hump curves were comparable with width and quartz peak positions, it was assumed that all samples would react similarly.

4. CONCLUSIONS

A guideline study was conducted using the experimental design program to investigate the impacts of six distinct variables on compressive strength, den-

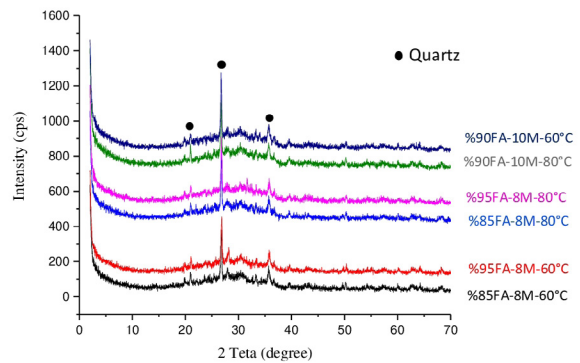


FIGURE 9. XRD analyses of samples made with various alkaline concentrations, curing temperatures, and fly ash concentrations.

sity, and thermal conductivity including fly ash-metakaolin ratio, alkalinity, curing temperature, calcium stearate, H_2O_2 , and expanded perlite. The study findings were statistically assessed, and the three most effective variables on density and strength were chosen, with ternary graphs made as a guide. The variation of thermal conductivity values was also analyzed with the help of contour plots. In this case, H_2O_2 and curing temperature were identified as the variables that had a combined effect on the strength and density values. Pearlite and alkaline concentration, respectively, were the third and fourth variables that influenced the strength and density values. The data for the technical needs stated in TS13655 were collected for non-load-bearing wall elements, and the working ranges that may be utilized as a guide were identified. Working with less than 1.75% H_2O_2 , a curing temperature greater than 70 $^\circ\text{C}$, an alkali concentration greater than 8 M, and expanded perlite less than 2.75% will match the predicted values when the operating ranges for both density and strength are examined together.

ACKNOWLEDGEMENTS

The authors wish to express their appreciation for financial support provided by individuals Afyon Kocatepe University under Grant number 19.Fen.Bil.01 as Scientific Research Project and also supported by TUBITAK under Grant number 218M778 for this work.

AUTHOR CONTRIBUTIONS:

Conceptualization: C. Kurtulus. Data curation: C. Kurtulus. Formal analysis: Investigation: C. Kurtulus. Methodology: C. Kurtulus, M. Serhat Baspınar. Project administration: C. Kurtulus, M. S. Baspınar. Supervision: C. Kurtulus, M. S. Baspınar. Validation: C. Kurtulus. Visualization: C. Kurtulus. Writing - original draft: C. Kurtulus. Review & editing: C. Kurtulus, M. S. Baspınar.

REFERENCES

- Vairagade, V.S.; Parbat, K.; Dhale, S.A. (2015) Fly ash as sustainable material for green concrete - A state of art. *Int. J.*

- Res. Eng. Sci. Technol.* 1 [2], 17–24.
- Dean, B.; Dulac, J.; Petrichenko, K.; Graham P. (2016) Towards a zero-emission, efficient, and resilient buildings and construction sector. *Global Status Report*. 1–48.
 - Jaya, N.A.; Yun-Ming, L.; Cheng-Yong H.; Abdullah, M.M.A.B.; Hussin K. (2020) Correlation between pore structure, compressive strength and thermal conductivity of porous metakaolin geopolymer. *Construc. Build. Mater.* 247, 118641. <https://doi.org/10.1016/j.conbuildmat.2020.118641>.
 - Rifaai, Y.; Yahia, A.; Mostafa, A.; Aggoun, S.; Kadri, E.H. (2019) Rheology of fly ash-based geopolymer: Effect of NaOH concentration. *Construc. Build. Mater.* 223, 583–94. <https://doi.org/10.1016/j.conbuildmat.2019.07.028>.
 - Cai, J.; Tan, J.; Li, X. (2020) Thermoelectric behaviors of fly ash and metakaolin based geopolymer. *Construc. Build. Mater.* 237, 117757. <https://doi.org/10.1016/j.conbuildmat.2019.117757>.
 - Singh, N.B.; Middendorf, B. (2020) Geopolymers as an alternative to Portland cement: An overview. *Construc. Build. Mater.* 237, 117455. <https://doi.org/10.1016/j.conbuildmat.2019.117455>.
 - Ling, Y.; Wang, K.; Wang, X.; Hua, S. (2019) Effects of mix design parameters on heat of geopolymerization, set time, and compressive strength of high calcium fly ash geopolymer. *Construc. Build. Mater.* 228, 116763. <https://doi.org/10.1016/j.conbuildmat.2019.116763>.
 - Wu, J.; Zhang, Z.; Zhang, Y.; Li, D. (2018) Preparation and characterization of ultra-lightweight foamed geopolymer (UFG) based on fly ash-metakaolin blends. *Construc. Build. Mater.* 168, 771–779. <https://doi.org/10.1016/j.conbuildmat.2018.02.097>.
 - Živica, V.; Palou, M.T.; Križma, M. (2015) Geopolymer cements and their properties: A review. *Build. Res. J.* 61 [2], 85–100. <https://doi.org/10.2478/brj-2014-0007>.
 - Singh, N.B. (2018) Foamed geopolymer concrete. *Mater. Today Proc.* 5 [7], 15243–15252. <https://doi.org/10.1016/j.matpr.2018.05.002>.
 - Srividya, T.; Kannan, P.R.; Sivasakthi, M.; Sujitha, A.; Jayalakshmi, R. (2022) A state-of-the-art on development of geopolymer concrete and its field applications. *Case Stud. Construc. Mater.* 16, e00812. <https://doi.org/10.1016/j.cscm.2021.e00812>.
 - Rashidi, S.; Esfahani, J.A.; Karimi, N. (2018) Porous materials in building energy technologies—A review of the applications, modelling and experiments. *Renew. Sustain. Energy Rev.* 91, 229–247. <https://doi.org/10.1016/j.rser.2018.03.092>.
 - Glasby, T.; Day, J.; Genrich, R.; Kemp, M. (2015) Commercial scale geopolymer concrete construction. The Saudi International Building and Constructions Technology Conference 1–11.
 - Dong, M.; Feng, W.; Elchalakani, M.; Li, G.K.; Karrech, A.; Sheikh, M.N. (2020) Material and glass-fibre-reinforced polymer bond properties of geopolymer concrete. *Mag. Concr. Res.* 72 [10], 509–525. <https://doi.org/10.1680/jmacr.18.00273>.
 - Aziz, I.H.; Al Bakri Abdullah, M.M.; Heah, C.Y.; Liew, Y.M. (2020) Behaviour changes of ground granulated blast furnace slag geopolymers at high temperature. *Adv. Cem. Res.* 32 [10], 465–475. <https://doi.org/10.1680/jacr.18.00162>.
 - Kalaiyarrasi, A.R.R.; Partheeban, P. (2019) Mechanical and microstructural properties of metakaolin geopolymer. *Emerg. Mater. Res.* 8 [2], 275–282. <https://doi.org/10.1680/jemmr.17.00019>.
 - Zhang, J.; Li, S.; Li, Z.; Gao, Y.; Liu, C.; Qi, Y. (2021) Workability and microstructural properties of red-mud-based geopolymer with different particle sizes. *Adv. Cem. Res.* 33 [5], 210–223. <https://doi.org/10.1680/jacr.19.00085>.
 - Dadsetan, S.; Siad, H.; Lachemi, M.; Sahmaran, M. (2019) Construction and demolition waste in geopolymer concrete technology: A review. *Mag. Concr. Res.* 71 [23], 1232–1352. <https://doi.org/10.1680/jmacr.18.00307>.
 - Davidovits, J. (2008) Geopolymer chemistry and applications. Institut Géopolymère, Saint-Quentin, (2008).
 - Giannopoulou, I.; Pania, D. (2007) Structure, design and applications of geopolymeric materials. Conference: 3rd Int. Conf. on Def. Pro. and Str. of Mat. 5–15.
 - Provis, J.L.; Deventer, S.J. (2014) Alkali activated materials state-of-the-art report, RILEM Melbourne, Australia, (2014).
 - Abdollahnejad, Z. (2016) Development of foam one-part geopolymers. Universidade do Minho, Portugal, (2016).
 - Lemougna, P.N.; Wang, K.-t.; Tang, Q.; Melo, U.C.; Cui, X.-m. (2016) Recent developments on inorganic polymers synthesis and applications. *Ceram. Int.* 42 [14], 15142–15159. <https://doi.org/10.1016/j.ceramint.2016.07.027>.
 - Provis, J.L.; Van Deventer, J.S.J. (2009) Geopolymers: structure, processing, properties and industrial applications. Woodhead Publishing, Cambridge, (2009).
 - Pacheco-torgal, F.; Lourenço, P.B.; Labrincha, J.A.; Kumar, S. (2014) Eco-efficient masonry bricks and blocks design, properties and durability. Woodhead Publishing, UK, (2014).
 - Ahmari, S.; Zhang, L. (2012) Production of eco-friendly bricks from copper mine tailings through geopolymerization. *Construc. Build. Mater.* 29, 323–331. <https://doi.org/10.1016/j.conbuildmat.2011.10.048>.
 - Schneider, M.; Romer, M.; Tschudin, M.; Bolio H. (2011) Sustainable cement production-present and future. *Cem. Concr. Res.* 41 [7], 642–650. <https://doi.org/10.1016/j.cemconres.2011.03.019>.
 - Ahmed, H.U.; Mohammed, A.A.; Rafiq, S.; Mohammed, A.S.; Mosavi A.; Sor N.H.; Qaidi, S.M.A. (2021) Compressive strength of sustainable geopolymer concrete composites: A state-of-the-art review. *Sustain.* 13 [24], 13502. <https://doi.org/10.3390/su132413502>.
 - Luhar, I.; Luhar, S.; Abdullah, M.M.A.B.; Razak, R.A.; Vizureanu, P.; Sandu, A.V.; Matasar, P.-D. (2021) A state-of-the-art review on innovative geopolymer composites designed for water and wastewater treatment. *Materials.* 14 [23], 7456. <https://doi.org/10.3390/ma14237456>.
 - Ghisellini, P.; Ripa, M.; Ulgiati, S. (2017) Exploring environmental and economic costs and benefits of a circular economy approach to the construction and demolition sector. A literature review. *J. Clean Product.* 178, 618–643. <https://doi.org/10.1016/j.jclepro.2017.11.207>.
 - Almutairi, A.L.; Tayeh, B.A.; Adesina, A.; Isleem, H.F.; Zeyad, A.M. (2021) Potential applications of geopolymer concrete in construction: A review. *Case Studies Construc. Mater.* 15, e00733. <https://doi.org/10.1016/j.cscm.2021.e00733>.
 - Malhotra, M.V. (2002) Introduction: sustainable development and concrete technology. *ACI Conc. Int.* 24 [7], 22.
 - Asadi, I.; Shafiq, P.; Abu Hassan, Z.F.B.; Mahyuddin, N.B. (2018) Thermal conductivity of concrete – A review. *J. Build. Eng.* 20, 81–93. <https://doi.org/10.1016/j.jobbe.2018.07.002>.
 - Yatsenko, E.A.; Goltsman, B.M.; Smolij, V.A.; Kosarev A.S. (2016) Investigation of a porous structure formation mechanism of a foamed slag glass based on the glycerol foaming mixture. *Res. J. Phar. Bio. Chem. Sci.* 7 [5], 1073–1081.
 - Abdollahnejad, Z.; Pacheco-Torgal, F.; de Aguiar, J.B. (2015) Development of foam one-part geopolymers with enhanced thermal insulation performance and low carbon dioxide emissions. *Adv. Mat. Res.* 1129, 565–572. <https://doi.org/10.4028/www.scientific.net/AMR.1129.565>.
 - Pacheco-Torgal, F. (2014) Eco-efficient construction and building materials research under the EU Framework Programme Horizon 2020. *Construc. Build. Mater.* 51, 151–162. <https://doi.org/10.1016/j.conbuildmat.2013.10.058>.
 - Bicer, A.; Kar, F. (2017) Thermal and mechanical properties of gypsum plaster mixed with expanded polystyrene and tragacanth. *Ther. Sci. Eng. Prog.* 1, 59–65. <https://doi.org/10.1016/j.tsep.2017.02.008>.
 - Singh, B.; Gupta, M.; Chauhan, M.; Bhattacharyya, S.K. (2020) Lightweight geopolymer concrete with EPS beads. *IOP Conf. Series. Mater. Sci. Engineer.* 869, 032048. <https://doi.org/10.1088/1757-899X/869/3/032048>.
 - Zhao, Y.; Jow, J.; Cai, X.; Lai, S. (2015) Fly ash-based geopolymer foam technology for thermal insulation and fire protection applications. World of Coal Ash (WOCA) Conference.
 - Zhang, Z.; Provis, J.L.; Reid, A.; Wang, H. (2014) Geopolymer foam concrete: An emerging material for sustainable construction. *Construc. Build. Mater.* 56, 113–127. <https://doi.org/10.1016/j.conbuildmat.2014.01.081>.

41. Pacheco-Torgal, F.; Jalali, S.; Fucic, A. (2012) Toxicity of building materials. Woodhead Publishing, USA, (2012).
42. Samson, G.; Cyr, M. (2017) Porous structure optimisation of flash-calcined metakaolin / fly ash geopolymer foam concrete geopolymer foam concrete. *Eur. J. Env. Civil Eng.* 22 [12], 1482-1498. <https://doi.org/10.1080/19648189.2017.1304285>.
43. Novais, R.M.; Pullar, R.C.; Labrincha, J.A. (2019) Geopolymer foams: An overview of recent advancements. *Progress Mat. Sci.* 109, 100621. <https://doi.org/10.1016/j.pmatsci.2019.100621>.
44. Yang, T.; Chou, C.; Chien, C. (2012) The effects of foaming agents and modifiers on a foamed-geopolymer. *Adv. Civil. Env. Mat. Res.* 905-914.
45. Bajare, D.; Vitola, L.; Dembovska, L.; Bumanis, G. (2019) Waste stream porous alkali activated materials for high temperature application. *Front. Mat.* 22 [6], 1-13. <https://doi.org/10.3389/fmats.2019.00092>.
46. Azimi, E.A.; Al Bakri Abdullah, M.M.; Ming, L.Y.; Yong, H.C.; Hussin, K.; Aziz, I.H. (2015) Review of geopolymer materials for thermal insulating applications. *Key Eng. Mater.* 660, 17-22. <https://doi.org/10.4028/www.scientific.net/KEM.660.17>.
47. Mattila, H. (2017) Moisture behavior of building insulation materials and good building practices. Conference: Rakennusfysiikka 2017 - Building Physics.
48. Vandanapu, S.N.; Krishnamurthy, M. (2018) Seismic performance of lightweight concrete structures. *Adv. Civil Eng.* 2018, 2105784. <https://doi.org/10.1155/2018/2105784>.
49. Vaou, V.; Panias, D. (2010) Thermal insulating foamy geopolymers from perlite. *Minerals Eng.* 23 [14], 1146-1151. <https://doi.org/10.1016/j.mineng.2010.07.015>.
50. Novais, R.M.; Buruberri, L.H.; Ascensão, G.; Seabra, M.P.; Labrincha, J.A. (2016) Porous biomass fly ash-based geopolymers with tailored thermal conductivity. *J. Clean Prod.* 119, 99-107. <https://doi.org/10.1016/j.jclepro.2016.01.083>.
51. Korat, L.; Ducman, V. (2017) The influence of the stabilizing agent SDS on porosity development in alkali-activated fly-ash based foams. *Cem. Conc. Comp.* 80, 168-174. <https://doi.org/10.1016/j.cemconcomp.2017.03.010>.
52. Cilla, M.S.; Morelli, M.R.; Colombo, P. (2014) Open cell geopolymer foams by a novel saponification/peroxide/gelcasting combined route. *J. Europ. Ceram. Soc.* 34 [12], 3133-3137. <https://doi.org/10.1016/j.jeurceramsoc.2014.04.001>.
53. Studart, A.R.; Gonzenbach, U.T.; Tervoort, E.; Gauckler, L.J. (2006) Processing routes to macroporous ceramics: A review. *J. Am. Cer. Soc.* 89 [6], 1771-1789. <https://doi.org/10.1111/j.1551-2916.2006.01044.x>.
54. Masi, G.; Rickard, W.D.A.; Vickers, L.; Bignozzi, M.C.; Van Riessen, A. (2014) A comparison between different foaming methods for the synthesis of light weight geopolymers. *Ceram. Int.* 40 [9], 13891-13902. <https://doi.org/10.1016/j.ceramint.2014.05.108>.
55. Medri, V.; Papa, E.; Dedecek, J.; Jirglova, H.; Benito, P.; Vaccari, A.; Landi, E. (2013) Effect of metallic Si addition on polymerization degree of in situ foamed alkali-aluminosilicates. *Ceram. Int.* 39 [7], 7657-7668. <https://doi.org/10.1016/j.ceramint.2013.02.104>.
56. Svingala, F.R. (2009) Alkali activated aerogels, Rochester Institute of Technology, Rochester (2009).
57. Gonzenbach, U.T.; Studart, A.R.; Tervoort, E.; Gauckler, L.J. (2006) Stabilization of foams with inorganic colloidal particles. *J. Am. Cer. Soc.* 22 [26], 10983-10988. <https://doi.org/10.1021/la061825a>.
58. Marvoto, A.; Setijadi, R.; Widyaningrum, A.; Waluyo, S. (2020) Drying shrinkage of concrete containing calcium stearate, $(Ca(C_{18}H_{35}O_2)_2)$, with ordinary Portland cement (OPC) as a binder: Experimental and modelling studies. *Molecules.* 25 [21], 4880. <https://doi.org/10.3390/molecules25214880>.
59. Nemat, C.M.; Naseroleslami, R.; Shekarchi, M. (2019) The impact of calcium stearate on characteristics of concrete. *Asian J. Civil Eng.* 20, 1007-1020. <https://doi.org/10.1007/s42107-019-00161-x>.
60. Maryoto, A. (2015) Improving microstructures of concrete using $Ca(C_{18}H_{35}O_2)_2$. *Procedia Eng.* 125, 631-637. <https://doi.org/10.1016/j.proeng.2015.11.086>.
61. Kurtulus, C.; Baspinar, M.S. (2020) Effect of calcium stearate on the thermal conductivity of geopolymer foam. *J. Turkish Chem. Soc.* 7 [2], 535-544. <https://doi.org/10.18596/jotesa.660727>.
62. Zhang, X.; Bai, C.; Qiao, Y.; Wang, X.; Jia, D.; Li, H.; Colombo, P. (2021) Porous geopolymer composites: A review. *Comp. Part A: App. Sci. Manufac.* 150, 106629.
63. Demir, İ.; Baspinar, S.; Kahraman, E. (2018) Production of insulations and construction materials from expanded perlite. *Lecture Notes Civil Eng.* 6, 24-32.
64. Sriwattanapong, M.; Sinsiri, T.; Pantawee, S. (2013) A study of lightweight concrete admixed with perlite. *Suranaree J. Sci. Technol.* 20 [3], 227-234.
65. Sengul, O.; Azizi, S.; Karaosmanoglu, F.; Tasdemir, M.A. (2011) Effect of expanded perlite on the mechanical properties and thermal conductivity of lightweight concrete. *Energy Build.* 43 [2-3], 671-676. <https://doi.org/10.1016/j.enbuild.2010.11.008>.
66. Chandra, S.; Berntsson, L. (2002) Lightweight aggregate, Noyes Publications, New York, (2002).
67. Gunasekara, C.M. (2016) Influence of properties of fly ash from different sources on the mix design and performance of geopolymer concrete, Engineering and Health RMIT University, Australia, (2016).
68. Tchakouté, H.K.; Rüscher, C.H. (2017) Mechanical and microstructural properties of metakaolin-based geopolymer cements from sodium waterglass and phosphoric acid solution as hardeners: A comparative study. *App. Clay Sci.* 140, 81-87. <https://doi.org/10.1016/j.clay.2017.02.002>.
69. De Vargas, A.S.; Dal Molin, D.C.C.; Vilela, A.C.F.; da Silva, F.J.; Pavão, B.; Veit, H. (2011) The effects of Na_2O/SiO_2 molar ratio, curing temperature and age on compressive strength, morphology and microstructure of alkali-activated fly ash-based geopolymers. *Cem. Conc. Comp.* 33 [6], 653-660. <https://doi.org/10.1016/j.cemconcomp.2011.03.006>.
70. Medri, V.; Papa, E.; Mazzocchi, M.; Laghi, L.; Morganti, M.; Francisconi, J.; Landi, E. (2015) Production and characterization of lightweight vermiculite/geopolymer-based panels. *Mater. Des.* 85, 266-274. <https://doi.org/10.1016/j.matdes.2015.06.145>.
71. Zhang, Z.; Wang, H. (2016) The pore characteristics of geopolymer foam concrete and their impact on the compressive strength and modulus. *Front. Mat.* 3, 38. <https://doi.org/10.3389/fmats.2016.00038>.
72. Bai, C.; Colombo, P. (2017) High-porosity geopolymer membrane supports by peroxide route with the addition of egg white as surfactant. *Ceram. Int.* 43 [2], 2267-2273. <https://doi.org/10.1016/j.ceramint.2016.10.205>.
73. Cui, Y.; Wang, D.; Zhao, J.; Li, D.; Ng, S.; Rui, Y. (2018) Effect of calcium stearate based foam stabilizer on pore characteristics and thermal conductivity of geopolymer foam material. *J. Build. Eng.* 20, 21-29. <https://doi.org/10.1016/j.jobe.2018.06.002>.
74. Bai, C.; Colombo, P. (2018) Processing, properties and applications of highly porous geopolymers: A review. *Ceram. Int.* 44 [14], 16103-16118. <https://doi.org/10.1016/j.ceramint.2018.05.219>.
75. Abdollahnejad, Z.; Nazari, A.; Pacheco-Torgal, F.; Sanjayan, J.G.; Barroso de Aguiar, J.L. (2015) Prediction of the compressive strength of one-part geopolymers. *Int. Conf Eng.* 1226-1234.
76. Shill, S.K.; Al-Deen, S.; Ashraf, M.; Hutchison, W. (2020) Resistance of fly ash based geopolymer mortar to both chemicals and high thermal cycles simultaneously. *Construc. Build. Mater.* 239, 117886. <https://doi.org/10.1016/j.conbuildmat.2019.117886>.
77. Kathirvel, P.; Kaliyaperumala, S.R.M. (2017) Probabilistic modeling of geopolymer concrete using response surface methodology. *Comput. Concr.* 19 [6], 737-744. <https://doi.org/10.12989/cac.2017.19.6.737>.
78. Ferreira, S.L.C.; Bruns, R.E.; Ferreira, H.S.; Matos, G.D.; David, J.M.; Brandão, G.C.; et al. (2007) Box-Behnken design: An alternative for the optimization of analytical methods. *Anal. Chim. Acta.* 597 [2], 179-186. <https://doi.org/10.1016/j.aca.2007.07.011>.

79. Li, N.; Shi, C.; Zhang, Z.; Zhu, D.; Hwang, H.J.; Zhu, Y.; Sun, T. (2018) A mixture proportioning method for the development of performance-based alkali-activated slag-based concrete. *Cem. Conc. Comp.* 93, 163–174. <https://doi.org/10.1016/j.cemconcomp.2018.07.009>.
80. Nazari, A.; Sanjayan, J.G. (2015) Hybrid effects of alumina and silica nanoparticles on water absorption of geopolymers: Application of Taguchi approach. *Measurement*. 60, 240–246. <https://doi.org/10.1016/j.measurement.2014.10.004>.
81. Hadi, M.N.S.; Zhang, H.; Parkinson, S. (2019) Optimum mix design of geopolymer pastes and concretes cured in ambient condition based on compressive strength, setting time and workability. *J. Build. Eng.* 23, 301–313. <https://doi.org/10.1016/j.jobe.2019.02.006>.
82. Lokuge, W.; Wilson, A.; Gunasekara, C.; Law, D.W.; Setunge, S. (2018) Design of fly ash geopolymer concrete mix proportions using multivariate adaptive regression spline model. *Construc. Build. Mater.* 166, 472–81. <https://doi.org/10.1016/j.conbuildmat.2018.01.175>.
83. Onoue, K.; Iwamoto, T.; Sagawa, Y. (2019) Optimization of the design parameters of fly ash-based geopolymer using the dynamic approach of the Taguchi method. *Construc. Build. Mater.* 219, 1–10. <https://doi.org/10.1016/j.conbuildmat.2019.05.177>.
84. ASTM C618-03 (2003) Standard specification for coal fly ash and raw or calcined natural pozzolan for use in concrete. Annu B ASTM Standard C, 3–6.
85. Luukkonen, T.; Abdollahnejad, Z.; Yliniemi, J.; Kinnunen, P.; Illikainen, M. (2018) One-part alkali-activated materials: A review. *Cem. Conc. Res.* 103, 21–34. <https://doi.org/10.1016/j.cemconres.2017.10.001>.
86. Görhan, G.; Aslaner, R.; Şinik, O. (2016) The effect of curing on the properties of metakaolin and fly ash-based geopolymer paste. *Compos. Part B. Eng.* 97, 329–335. <https://doi.org/10.1016/j.compositesb.2016.05.019>.
87. Izaguirre, A.; Lanas, J.; Alvarez, J.I. (2009) Effect of water-repellent admixtures on the behaviour of aerial lime-based mortars. *Cem. Conc. Res.* 39 [11], 1095–1104. <https://doi.org/10.1016/j.cemconres.2009.07.026>.
88. Ranjbar, N.; Talebian, S.; Mehrali, M.; Kuenzel, C.; Cornelis, M.H.S.; Jumaat, M.Z. (2016) Mechanisms of interfacial bond in steel and polypropylene fiber reinforced geopolymer composites. *Composites Sci. Tech.* 122, 73–81. <https://doi.org/10.1016/j.compscitech.2015.11.009>.
89. Abdollahnejad, Z.; Mastali, M.; Dalvand, A. (2017) Comparative study on the effects of recycled glass-fiber on drying shrinkage rate and mechanical properties of the self-compacting mortar and fly ash-slag geopolymer mortar. *J. Mat. Civil Eng.* 29 [8], 1–11. [https://doi.org/10.1061/\(ASCE\)MT.1943-5533.0001918](https://doi.org/10.1061/(ASCE)MT.1943-5533.0001918).
90. Ranjbar, N.; Zhang, M. (2020) Fiber-reinforced geopolymer composites: A review. *Cem. Conc. Comp.* 107, 103498. <https://doi.org/10.1016/j.cemconcomp.2019.103498>.
91. Sukontasukkul, P.; Pongsopha, P.; Chindaprasit, P.; Songpiriyakij, S. (2018) Flexural performance and toughness of hybrid steel and polypropylene fibre reinforced geopolymer. *Construc. Build. Mater.* 161, 37–44. <https://doi.org/10.1016/j.conbuildmat.2017.11.122>.
92. Mastali, M.; Kinnunen, P.; Dalvand, A.; Mohammadi Firouz, R.; Illikainen, M. (2018) Drying shrinkage in alkali-activated binders—A critical review. *Construc. Build. Mater.* 190, 533–550. <https://doi.org/10.1016/j.conbuildmat.2018.09.125>.
93. Kheradmand, M.; Abdollahnejad, Z.; Pacheco-Torgal, F. (2020) Drying shrinkage of fly ash geopolymeric mortars reinforced with polymer hybrid fibres. *Proc. Inst. Civ. Eng. Constr. Mater.* 173 [1], 28–40. <https://doi.org/10.1680/jcoma.16.00077>.
94. Amran, Y.H.M.; Farzadnia, N.; Ali, A.A.A. (2015) Properties and applications of foamed concrete; a review. *Construc. Build. Mater.* 101 [1], 990–1005. <https://doi.org/10.1016/j.conbuildmat.2015.10.112>.
95. Jedidi, M.; Benjeddou, O.; Soussi, C. (2015) Effect of expanded perlite aggregate dosage on properties of lightweight concrete. *Jordan J. of Civ. Eng.* 9 [3], 278–291. <https://doi.org/10.14525/jjce.9.3.3071>.
96. Hardjito, D.; (2005) Development and properties of low-calcium fly ash-based geopolymer concrete, Curtin University of Technology, Australia, (2005).
97. Tsaousi, G.M.; Douni, I.; Panias, D. (2016) Characterization of the properties of perlite geopolymer pastes. *Mater. Construc.* 66 [324], e102. <https://doi.org/10.3989/mc.2016.10415>.
98. ASTM C332-17 (2017) Standard specification for lightweight aggregates for insulating concrete.
99. ASTM C330 (2017) Standard specification for lightweight aggregates for structural concrete, Annual book of ASTM Standards.
100. Hardjito, D.; Wallah, S.E.; Sumajouw, D.M.J. Rangan, B.V. (2004) On the development of fly ash-based geopolymer concrete. *Am. Conc. Instit. Mater. J.* 101 [6], 467–472.
101. Feng, J.; Zhang, R.; Gong, L.; Li, Y.; Cao, W.; Cheng, X. (2015) Development of porous fly ash-based geopolymer with low thermal conductivity. *Mater. Des.* 65, 529–533. <https://doi.org/10.1016/j.matdes.2014.09.024>.
102. Zhu, M.; Ji, R.; Li, Z.; Wang, H.; Liu, L.L.; Zhang, Z. (2016) Preparation of glass ceramic foams for thermal insulation applications from coal fly ash and waste glass. *Construc. Build. Mater.* 112, 398–405. <https://doi.org/10.1016/j.conbuildmat.2016.02.183>.
103. Jaya, N.A.; Yun-Ming, L.; Cheng-Yong, H.; Abdullah, M.M.A.B.; Hussin, K. (2020) Correlation between pore structure, compressive strength and thermal conductivity of porous metakaolin geopolymer. *Construc. Build. Mater.* 247, 118641. <https://doi.org/10.1016/j.conbuildmat.2020.118641>.
104. Sumirat, I.; Ando, Y.; Shimamura, S. (2006) Theoretical consideration of the effect of porosity on thermal conductivity of porous materials. *J. Porous Mater.* 13, 439–443. <https://doi.org/10.1007/s10934-006-8043-0>.
105. Skibinski, J.; Cwieka, K.; Ibrahim, S.H.; Wejrzanowski, T. (2019) Influence of pore size variation on thermal conductivity of open-porous foams. *Materials*. 12 [12], 2017. <https://doi.org/10.3390/ma12122017>.
106. Demirboğa, R.; Gül, R. (2003) The effects of expanded perlite aggregate, silica fume and fly ash on the thermal conductivity of lightweight concrete. *Cem. Conc. Res.* 33 [5], 723–727. [https://doi.org/10.1016/S0008-8846\(02\)01032-3](https://doi.org/10.1016/S0008-8846(02)01032-3).
107. Karaaslan, C.; Yener, E. (2021) The effect of alkaline activator components on the properties of fly ash added pumice based geopolymer. *J. Inst. Sci. Technol.* 11 [2], 1255–1269. <https://doi.org/10.21597/jist.840872>.
108. Jaya, N.A.; Yun-Ming, L.; Abdullah, M.M.A.B.; Cheng-Yong, H.; Hussin, K. (2018) Effect of sodium hydroxide molarity on physical, mechanical and thermal conductivity of metakaolin geopolymers. *IOP Conf. Ser. Mater. Sci. Eng.* 343, 012015. <https://doi.org/10.1088/1757-899X/343/1/012015>.
109. Kadoi, K.; Nakae, H. (2011) Relationship between foam stabilization and physical properties of particles on aluminum foam production. *Mater. Trans.* 52 [10], 1912–1919. <https://doi.org/10.2320/matertrans.F-M2011817>.
110. Gu, G.; Xu, F.; Huang, X.; Ruan, S.; Peng, C.; Lin, J. (2020) Foamed geopolymer: The relationship between rheological properties of geopolymer paste and pore-formation mechanism. *J. Clean Prod.* 277, 123238. <https://doi.org/10.1016/j.jclepro.2020.123238>.
111. Puertas, F.; Torres-Carrasco, M. (2014) Use of glass waste as an activator in the preparation of alkali-activated slag. Mechanical strength and paste characterisation. *Cem. Conc. Res.* 57, 95–104. <https://doi.org/10.1016/j.cemconres.2013.12.005>.
112. Tchakouté, H.K.; Rüscher, C.H.; Kong, S.; Kamseu, E.; Leonelli, C. (2016) Geopolymer binders from metakaolin using sodium waterglass from waste glass and rice husk ash as alternative activators: A comparative study. *Construc. Build. Mater.* 114, 276–89. <https://doi.org/10.1016/j.conbuildmat.2016.03.184>.
113. Monich, P.R.; Romero, A.R.; Höllen, D.; Bernardo, E. (2018) Porous glass-ceramics from alkali activation and sinter-crystallization of mixtures of waste glass and residues from plasma processing of municipal solid waste. *J. Clean. Prod.* 188, 871–878. <https://doi.org/10.1016/j.jclepro.2018.03.167>.
114. Husain, S.; Permittaria, A.; Haryanti, N.H.; Suryajaya, S. (2019) Effect calcination temperature on formed of calcium silicate from rice husk ash and snail shell. *J. Neutrino. J. Fisika dan Apl.* 11 [2], 45–51.
115. Abdulkareem, O.A. (2017) Effects of high activator content on fly ash-based geopolymers exposed to elevated temperatures. *J. Mater. Appl.* 6 [1], 1–12.

Appendix 1. Variables used in experiment design and analysis results.

No	Fly ash (%)	Metakaolin (%)	Ca-Stearate (%)	Expanded perlite (%)	Alkaline concentration (M)	H ₂ O ₂ (%)	Curing temperature (°C)	Compressive strength (MPa)	Density (kg/m ³)
1	85	15	0,45	0	6	1,5	70	1,59	450
2	85	15	0,45	0	10	1,5	70	1,672	540
3	95	5	0,45	0	6	1,5	70	0,676	432
4	95	5	0,45	0	10	1,5	70	1,779	567
5	85	15	0,45	20	6	1,5	70	0,576	445
6	85	15	0,45	20	10	1,5	70	1,668	527
7	95	5	0,45	20	6	1,5	70	1,605	473
8	95	5	0,45	20	10	1,5	70	1,505	475
9	85	15	0,15	10	8	1,5	60	1,451	515
10	95	5	0,15	10	8	1,5	60	1,455	452
11	85	15	0,75	10	8	1,5	60	1,014	431
12	95	5	0,75	10	8	1,5	60	2,018	528
13	85	15	0,15	10	8	1,5	80	1,192	472
14	95	5	0,15	10	8	1,5	80	1,125	435
15	85	15	0,75	10	8	1,5	80	1,191	481
16	95	5	0,75	10	8	1,5	80	1,481	458
17	90	10	0,15	0	8	1	70	2,612	537
18	90	10	0,75	0	8	1	70	2,656	563
19	90	10	0,15	20	8	1	70	1,304	526
20	90	10	0,75	20	8	1	70	0,578	465
21	90	10	0,15	0	8	2	70	1,794	432
22	90	10	0,75	0	8	2	70	1,259	415
23	90	10	0,15	20	8	2	70	0,623	344
24	90	10	0,75	20	8	2	70	1,119	385
25	90	10	0,45	0	6	1,5	60	1,44	475
26	90	10	0,45	0	10	1,5	60	1,864	560
27	90	10	0,45	20	6	1,5	60	1,22	450
28	90	10	0,45	20	10	1,5	60	2,011	535
29	90	10	0,45	0	6	1,5	80	0,658	414
30	90	10	0,45	0	10	1,5	80	1,872	472
31	90	10	0,45	20	6	1,5	80	1,61	475
32	90	10	0,45	20	10	1,5	80	1,208	480
33	85	15	0,45	10	8	1	60	2,485	568
34	95	5	0,45	10	8	1	60	2,747	566
35	85	15	0,45	10	8	1	80	1,196	461
36	95	5	0,45	10	8	1	80	2,006	567
37	85	15	0,45	10	8	2	60	1,152	398
38	95	5	0,45	10	8	2	60	1,203	382
39	85	15	0,45	10	8	2	80	0,682	367
40	95	5	0,45	10	8	2	80	0,732	378

No	Fly ash (%)	Metakaolin (%)	Ca-Stearate (%)	Expanded perlite (%)	Alkaline concentration (M)	H ₂ O ₂ (%)	Curing temperature (°C)	Compressive strength (MPa)	Density (kg/m ³)
41	90	10	0,15	10	6	1	70	2,61	557
42	90	10	0,15	10	10	1	70	2,15	590
43	90	10	0,75	10	6	1	70	2,109	511
44	90	10	0,75	10	10	1	70	2,134	592
45	90	10	0,15	10	6	2	70	1,576	394
46	90	10	0,15	10	10	2	70	1,864	432
47	90	10	0,75	10	6	2	70	1,22	367
48	90	10	0,75	10	10	2	70	2,011	425
49	90	10	0,45	10	8	1,5	70	1,8	535
50	90	10	0,45	10	8	1,5	70	1,8	444
51	90	10	0,45	10	8	1,5	70	1,8	445
52	90	10	0,45	10	8	1,5	70	1,8	450
53	90	10	0,45	10	8	1,5	70	1,8	449
54	90	10	0,45	10	8	1,5	70	1,8	457